infrastructures

MDPI

Article

Evaluation of Damage to Existing Buildings Induced by Tunnel Excavation

Ekin Evrim Laçin Akşit * and Kadir Güler

Department of Civil Engineering, Istanbul Technical University, Ayazağa Campus, 34469 Istanbul, Türkiye; kguler@itu.edu.tr

* Correspondence: lacine@itu.edu.tr

Abstract: This study emphasizes the significance of employing systematic approaches and precise modeling techniques to evaluate potential building damage from metro tunnel excavations. Mair et al. (1996) proposed a three-stage assessment framework comprising preliminary assessment, second-stage assessment, and detailed assessment to analyze the damage to buildings inflicted by tunnel excavation. For preliminary and second-stage assessments, parametric calculation methods have been examined; however, detailed assessment requires using a 3D numerical analysis model. This study selected a school building, to examine this three-stage assessment method. For the preliminary and second stage assessments, a "greenfield" analysis approach was utilized using the PLAXIS 2D to determine the ground settlement curve caused by tunnel excavation. Based on the obtained settlement values, the evaluation was conducted using the boundary conditions proposed by Mair et al. (1996). Since the obtained settlement values did not meet the proposed boundary conditions, a three-dimensional finite element model was generated using the SAP2000 analysis program. This paper offers practical guidance on the nonlinear modeling principles of structural elements during the detailed assessment of a building subjected to vertical settlement. It provides a framework for assessing buildings near tunnel construction sites.

Keywords: tunnel effects; ground settlement; building damage

Academic Editor: Jorge de Brito

Received: 4 November 2024
Revised: 8 December 2024
Accepted: 20 December 2024
Published: 9 January 2025

Citation: Laçin Akşit, E.E.; Güler, K. Evaluation of Damage to Existing Buildings Induced by Tunnel Excavation. *Infrastructures* **2025**, *10*, 13. https://doi.org/10.3390/infrastructures10010013

1. Introduction

The construction of metro tunnels, which provides a solution to urban traffic congestion, is on the rise globally. The ground surface movement caused by tunnel excavation poses a risk of damage and collapse to structures along the route. Predicting ground movements and the resultant structural deformations is crucial in mitigating the risk of building damage [1–3].

Research on the effects of metro tunnel excavation on existing structures is growing as expertise in the field expands. The surface settlement caused by metro tunnel excavations is contingent upon the ground loss, which is influenced by ground/rock conditions and excavation methods. When a gap is suddenly created in the ground without an equivalent rigid cover to fill it, deformations may occur within the tunnel depth. These deformations are referred to as "ground loss", an empirical expression determined by ground conditions [3–5].

Complex numerical analysis models can be developed to predict potential damage to critical structures along the metro tunnel route [6,7]. However, detailed numerical analysis models could be more practical for evaluating hundreds of buildings along the metro

tunnel route during the preliminary design stage [3,8]. For this reason, Mair et al. (1996) [9] proposed a three-stage assessment method, including preliminary assessment, second-stage assessment, and detailed assessment, to be utilized in the preliminary design phase. Predicting the ground movements induced by tunneling is essential for assessing the impact on structures. Various methods have been proposed to predict the ground displacements resulting from tunnel construction.

In preliminary assessment, vertical displacement contours are generated, enabling the determination of each building's vertical displacement and settlement slope. The effect of the building stiffness on the settlement, termed "greenfield settlement", is neglected. If the vertical displacement is less than 10 mm and the settlement slope is less than 1:500, the building is deemed to have negligible damage. Recent studies, however, have observed that the effects of ground movements may significantly change when structural stiffness is considered. The preliminary assessment stage tends to be overly conservative due to neglect of building stiffness.

In the second-stage assessment, maximum tensile strains including the bending and diagonal strains of the building are calculated. The building is modeled as an elastic beam conforming to the "greenfield settlement", while ignoring building stiffness. The third stage assessment becomes necessary if the damage category is moderate or greater. Since building stiffness is still neglected, the second assessment stage is also overly conservative. Detailed evaluation is based on the principle of three-dimensional numerical analysis using finite element method-based software, which allows a more nuanced examination of the structural behavior and is crucial for an accurate understanding of the safety and stability of buildings or tunnels. Instrumental observations are conducted in the third stage assessment, monitoring the structure and ground behavior during tunnel construction and the service stage.

This paper investigates the parametric and numerical calculations of the three-stage approach proposed by Mair et al. (1996) [9], focusing on its effectiveness in the process of structural evaluation. This study focused on the evaluation process for a building located along a tunnel route during excavation. The literature has lacked detailed information regarding the principles of creating a numerical model for a building under vertical settlement. This study, which examines the assessment process for buildings affected by tunnel excavation, has three main objectives: to investigate the parametric calculation methods, to determine the three-dimensional modeling principles for a building analyzed in the detailed assessment phase, and to develop the vertical pushover analysis approach to be applied to the three-dimensional analysis model. The effectiveness of this approach in investigating building behavior is highlighted, with comprehensive information provided on how these principles should be employed to monitor structural behavior during the tunnel construction and service periods. Detailed numerical analyses have been conducted; the results are presented in tables and figures for comparative purposes.

2. Materials and Methods

The surface settlement resulting from tunnel excavations is described by the semi-empirical "Gaussian curve" theory, initially proposed by Peck and Schmidt (1969) [10,11]. This method calculates the ground movement perpendicular to the tunnel axis. The presence of the existing buildings on the ground surface and their proximity to the tunnel can influence the development of ground movement. However, before considering the complexities of an existing building, it is crucial to understand the settlements influenced solely by the tunnel ("greenfield" ground movement). For this purpose, a semi-empirical Gaussian curve representing long-term "greenfield" settlements was obtained, derived from more than 20 case histories by Peck (1969) (Figure 1) [12].

The Gaussian curve is a distribution curve resulting from numerous field measurements. The equations defining this curve are presented in Equations (1)–(4) [9]. The equation of the Gaussian curve is expressed as S. The S_{max} value indicates the maximum settlement along the tunnel axis, x is the horizontal distance from the center line, z_0 is the distance of the tunnel axis to the ground surface, K is the trough width parameter, i is the horizontal distance of the settlement curve inflection point to the tunnel centerline, V_L is the volume loss, vs. is the volume of the settlement trough, and D is the tunnel diameter.

$$S = S_{max} e^{\left(\frac{-x^2}{2i^2}\right)} \tag{1}$$

$$i = Kz_0 \tag{2}$$

$$V_L = \frac{4V_s}{\pi D^2} \tag{3}$$

$$S_{max} = \frac{0.313 V_L D^2}{i} \tag{4}$$

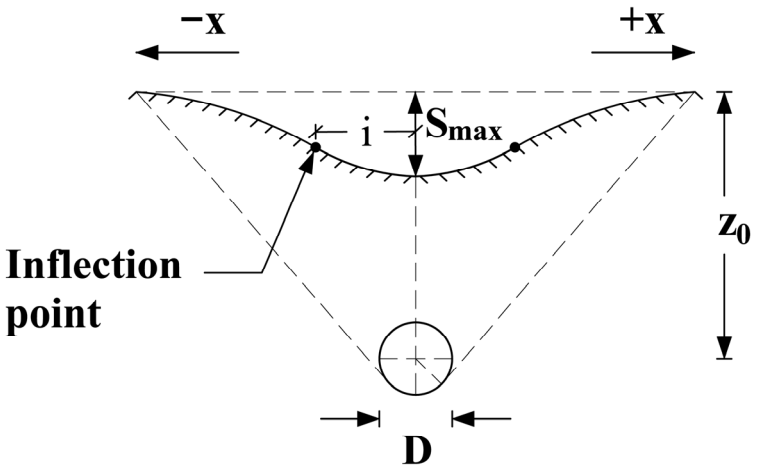

Figure 1. Transverse direction surface settlement curve (Gaussian curve).

The slope of the Gaussian curve represents the slope between two selected points on the curve, reaching its maximum value at the inflection point. This parameter is vital for evaluating the structural behavior of buildings, as it determines the relative vertical movement between two points on the structure.

The three-stage approach method outlined by Mair et al. (1996) is employed during the preliminary design phase to assess potential damage to structures due to tunnel excavations (Figure 2) [9]. The preliminary evaluation relies on "greenfield" settlement and settlement slope values. Contours corresponding to calculated surface settlements are drawn on a plan view containing the buildings along the route. Each structure's settlement and settlement slope values are determined using these contours. Structures experiencing maximum settlement of less than 10 mm and maximum settlement slope of less than 1:500 are considered sufficiently safe and excluded from further assessment. If these thresholds are exceeded, the second-stage assessment is initiated.

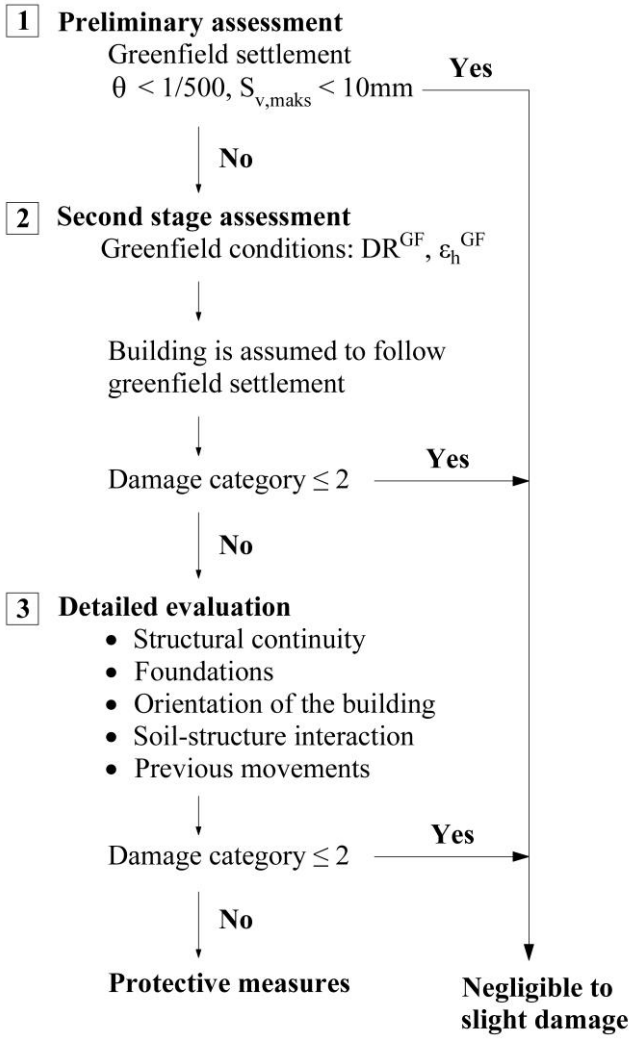

Figure 2. Three-stage damage assessment approach proposed by Mair et al. (1996) [9].

In the second-stage assessment, the interaction between soil and structure is considered, estimating bending and diagonal strains on the building. This approach is conservative as it ignores the building stiffness, assuming it conforms to the "greenfield" settlement curve. In reality, the building's stiffness tends to reduce both the settlement rates and the horizontal strain. Therefore, the damage category determined in the second-stage assessment often exceeds the actual damage levels.

The methodology for determining the building's unit tensile strain (ε_{max}) takes the equivalent beam approach as a basis [13]. In this model, the structure is represented as a rectangular cross-section beam subjected to sagging and hogging deformation modes, considered weightless and elastic (Figure 3) [14]. This approach provides insight into crack formation mechanisms and calculates critical unit strain values. The critical unit strain is the greater strain caused by bending (ε_b) and shear effects (ε_d). The horizontal unit strain (ε_h) is defined as the average strain due to the relative horizontal movement at either end of a building span, reaching its maximum value at the inflection point, thereby influencing the compression or tension behavior of the structure. Consequently, it plays a crucial role in evaluating structural behavior.

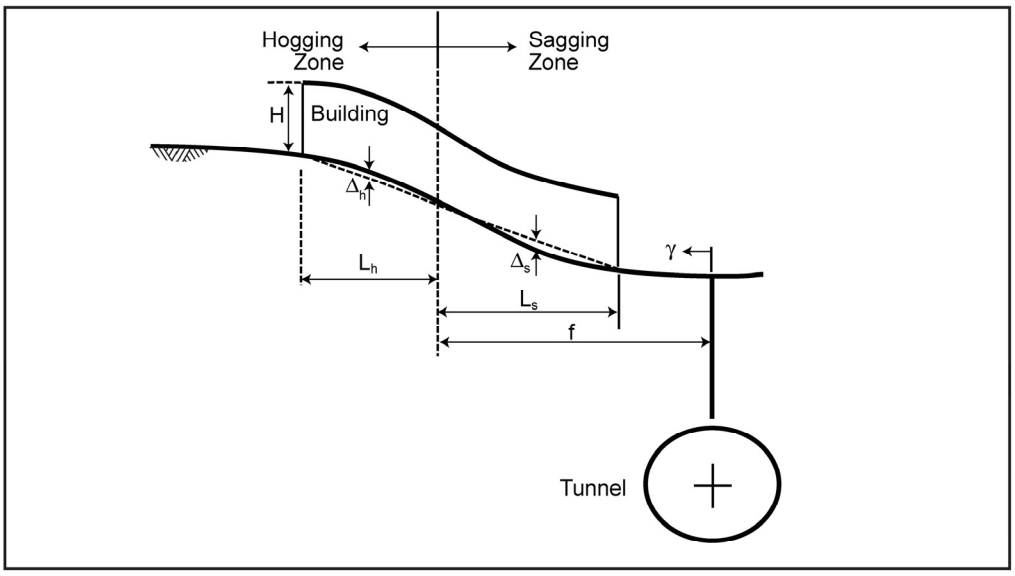

Figure 3. Equivalent beam model for a structure under hogging and sagging effects.

Bending and shear behavior are considered alongside sagging and hogging effects, allowing for the calculation of unit strains in each case (Equations (5) and (6)) [9], where L is the length of the hogging or sagging region, H is the building height, Δ is the relative vertical deflection, I is the moment of inertia of the equivalent beam ($H^3/12$ for the sagging region, $H^3/3$ for the hogging region), and t is the furthest distance from the neutral axis to the edge of the beam ($H/2$ for the sagging region, H for the hogging region). The E/G ratio is the relationship between Young's modulus and shear modulus of the building. This ratio varies by building type, with values of 2.6 for load-bearing masonry walls, 12.5 for reinforced concrete frame structures, and 0.5 for rigid masonry structures.

$$\frac{\Delta}{L} = \left(\frac{L}{12t} + \frac{3I}{2tLH}\frac{E}{G}\right)\varepsilon_b \tag{5}$$

$$\frac{\Delta}{L} = \left(1 + \frac{HL^2}{18I}\frac{G}{E}\right)\varepsilon_d \tag{6}$$

The maximum unit tensile strain (ε_{max}) is calculated from Equation (7) [9], where ε_{bt} is the total bending strain and ε_{dt} is the diagonal distortion.

$$\varepsilon_{max} = max(\varepsilon_{bt}; \varepsilon_{dt}) \tag{7}$$

$$\varepsilon_{bt} = \varepsilon_h + \varepsilon_b \tag{8}$$

$$\varepsilon_{dt} = 0.35\varepsilon_h + \sqrt{(0.65\varepsilon_h)^2 + \varepsilon_d^2} \tag{9}$$

The calculated ε_{max} value is compared with the limits in Table 1 [9] to define the category of structural damage [12]. If the damage category exceeds 2, further detailed evaluation is conducted. The structural damage determination method used for rapid assessment of damage, based on angular distortion and horizontal strain was illustrated [15].

Table 1. Relationship between the category of damage and limiting tensile strain.

Category of Damage	Normal Degree of Severity	Limiting Tensile Strain (ε_{max}) (%)
0	Negligible	0–0.05
1	Very slight	0.05–0.075
2	Slight	0.075–0.15
3	Moderate	0.15–0.3
4–5	Severe to very severe	>0.3

The detailed assessment begins with a site visit for visual inspection and evaluation of building stiffness, current conditions, and potential damage outcomes. These examinations define the building's risk based on numerical analysis principles, using finite element method-based software. Following the detailed assessment results, protective measures are recommended for buildings classified with moderate or severe damage to minimize collapse risk or control their structural response. These buildings will undergo a thorough inspection and intensive monitoring, considering both building and ground stiffness, following the principles established by [16].

2.1. An Inspection of an Existing Building on the Metro Tunnel Route

During metro tunnel excavations, vertical settlement in the ground due to the volume loss impacts buildings along the route. The studies presented in the literature provide insights into the damage levels these vertical settlements may create. An existing school building on the metro tunnel route was examined according to the assessment approach recommended by Mair et al. (1996) [9]. Figure 4 displays the school building's location relative to the tunnel.

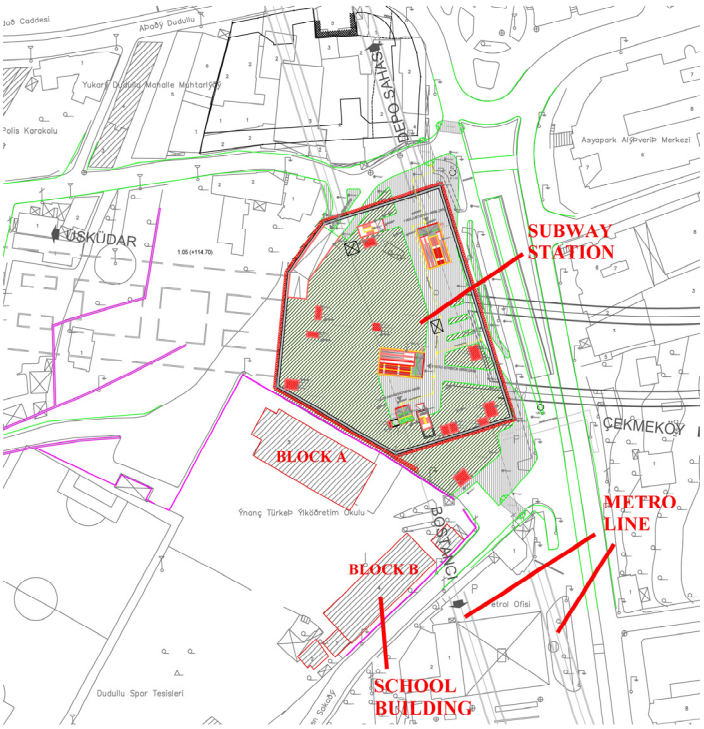

Figure 4. Location of the school building.

The subway station to be excavated on the metro tunnel route is a tunnel-type station consisting of an N1 shaft and P1, B2, B3, and B5-type tunnels. The most critical tunnel type affecting the relevant school building during this tunnel construction is the B5-type tunnel (Figure 5). Therefore, a "greenfield" analysis model of the B5 tunnel section (the

section where the B5-type tunnel is located between the P1-type tunnels) was created using PLAXIS 2D. Within the scope of the application project, one borehole numbered GMD11-01 was established. The drilled borehole revealed clay and limestone units in the section where the station is located (Table 2) [17]. The measurements indicate that the water level is approximately 8.00 m below the excavation level [17].

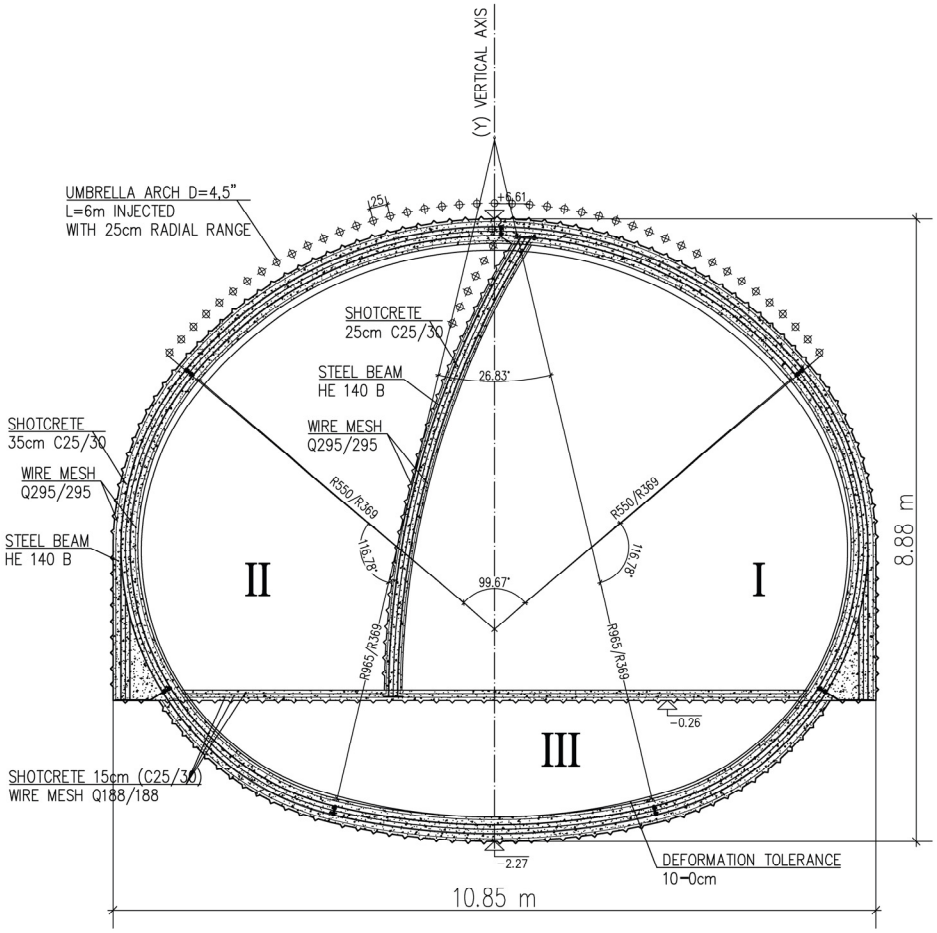

Figure 5. B5-type tunnel section.

Table 2. Soil parameters used in the analysis.

Lithology	E (kPa)	C (kPa)	θ (°)	ν	γ (kN/m^3)
Clay	40,000	0	30	0.33	20
Limestone	675,000	141	38	0.28	26

The depth of the B5 tunnel, selected as the most critical section for the "greenfield" analysis, was found to be 31.00 m. The PLAXIS 2D analysis model for the "greenfield" condition is presented in Figure 6. For the analysis model, soil stratigraphy was defined, and the geometry of the analysis model was created by defining the boreholes. Structural components such as tunnels were modeled. The "Tunnel Designer" feature was used to model the tunnel section. The geometry of the tunnel section was created, and the parameters of the tunnel supports were assigned. The mesh properties were defined, and the geometry model was discretized and transformed into a finite element model. In this model, the element distribution level was selected as "very fine", with a relative element size factor (r_e) of 0.50 (500–1250 elements). In this model, the side edges were defined as X-fixed and Y-free; both directions were fixed at the bottom, and both directions were defined as free at the top.

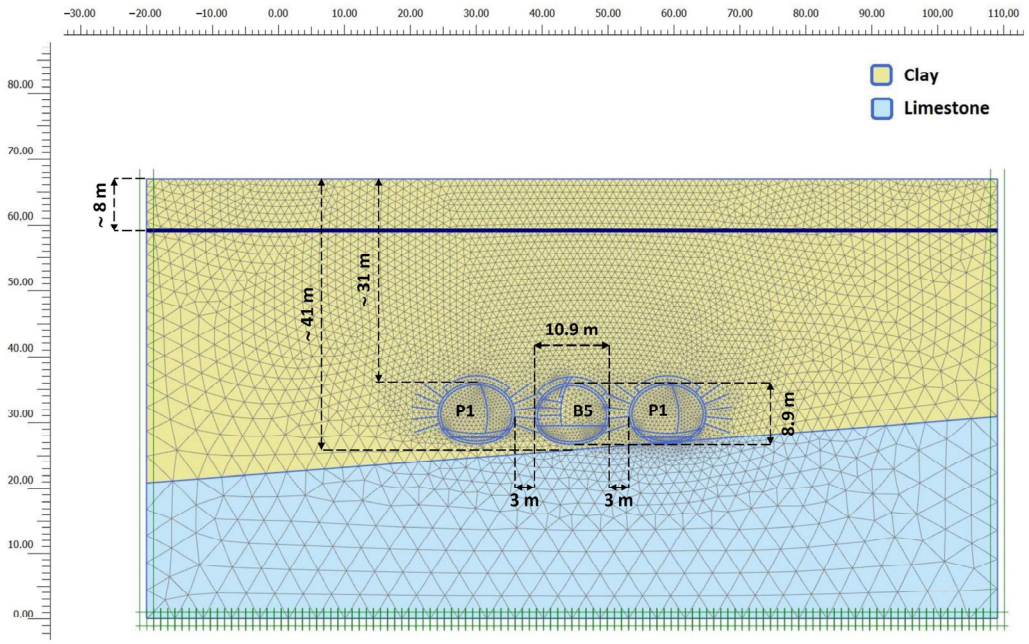

Figure 6. The PLAXIS 2D model for B5-type tunnel section.

The Plaxis2D model for the preliminary assessment was created via the "greenfield" analysis approach. Figure 7 illustrates cross-section used for the Plaxis2D model. This cross-section, perpendicular to the tunnel axis, diagonally intersects the school building for a length of 39.00 m. Vertical displacements on the ground surface due to volume loss during tunnel excavation were obtained along this length. Since the building stiffness was not considered during the assessment of vertical displacement, the values derived from the Plaxis2D model remained conservative compared with the actual values. The maximum vertical displacement value obtained was 79 mm. According to Mair et al. (1996) [9], the maximum allowable settlement for the preliminary evaluation stage is 10 mm. The second-stage evaluation was necessary because the "greenfield" analysis result exceeded this threshold.

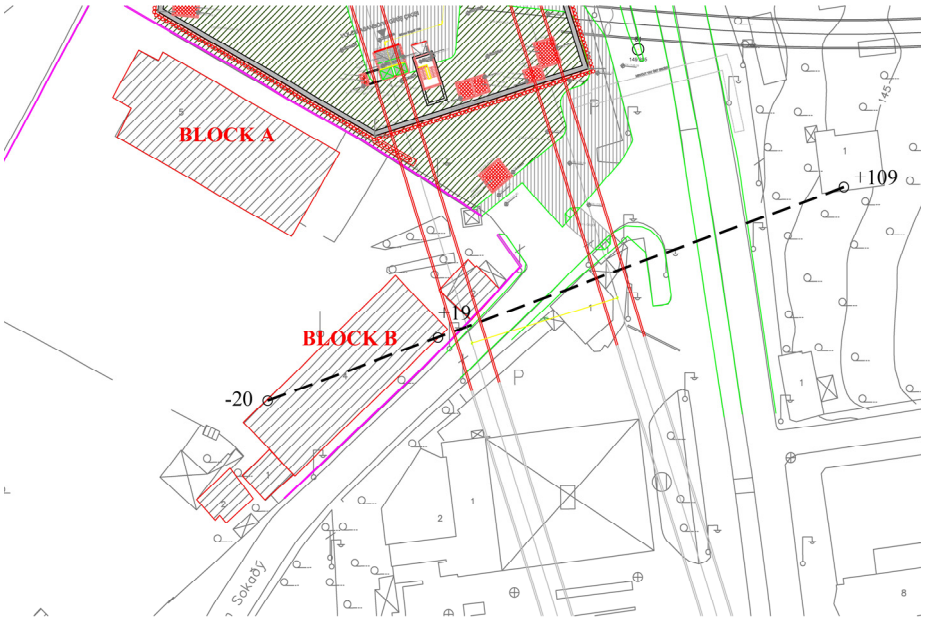

Figure 7. Cross-section used for "greenfield" analysis.

In the second-stage assessment, the building was assumed to conform to the curve obtained from the "greenfield" analysis in the preliminary assessment phase. Based on this curve, hogging and sagging zones were identified, as depicted in Figure 8. The tensile strain control was performed by considering the maximum unit strain values in both the hogging and sagging zones of the building (Equation (7), Table 3).

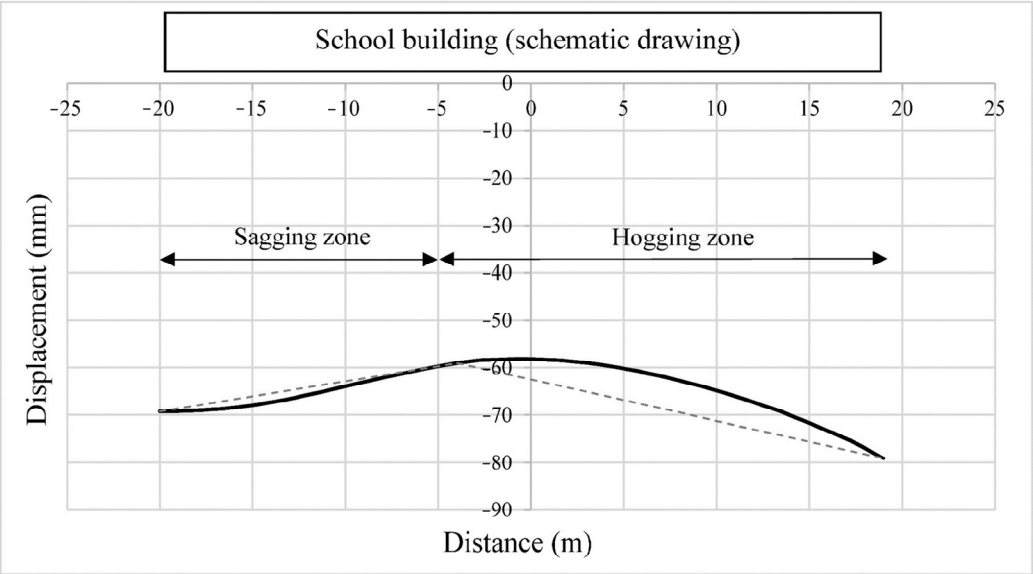

Figure 8. The settlement curve illustrating the displacements occurring beneath the school building during the tunnel construction, based on "greenfield" analysis.

Table 3. The unit strain control in the hogging and sagging zones of the school building.

	Sagging Zone	**Hogging Zone**
L (m)	16	23
Δ (mm)	1.82	6.74
t (m)	4.80	9.60
I (m^4)	73.73	294.91
ε_b (%)	0.005	0.010
ε_d (%)	0.010	0.027
ε_h (%)	0.288	0.218
ε_{bt} (%)	0.294	0.228
ε_{dt} (%)	0.288	0.220
ε_{max} (%)	0.294	0.228

The maximum strain value (ε_{max}) obtained in Table 3 was compared with the limit tensile strain values provided by Boscardin and Cording (Table 1). In the second-stage assessment of the school building, the damage category was classified as 3, indicating a "moderate" level of damage. As previously mentioned, since the damage category exceeded 2, a detailed assessment of the school building was initiated.

In the detailed assessment phase, a SAP2000 analysis model was developed to evaluate the damage to the school buildings and the effects of vertical settlement. This model incorporated the vertical settlements observed in the field after excavation, enabling an examination of the damages sustained by the school building. The objective was to determine the principles of the finite element analysis model utilized in the detailed assessment stage.

For the numerical treatment, the previously retrofitted school building was considered. The information about the building was sourced from the retrofit report issued in 2012 [18]. The school building consists of two blocks called A and B, with block B being the focus of this investigation. Block B was constructed in 1977; it comprises a ground floor and two

additional floors. Its structural system consists of reinforced concrete frames and shear walls, with story heights of 3.20 m. The floor plan dimensions are 43.75 m by 15.05 m in the long and short directions, respectively. The average concrete compressive strength was 10 MPa, according to compression tests conducted on core samples and non-destructive surface hardness tests (Schmidt hammer). The reinforcement steel used in the building was S220 grade, plain reinforcement. The superstructure loads are transferred to the soil via a strip foundation. The architectural cross-section of the school building is depicted in Figure 9.

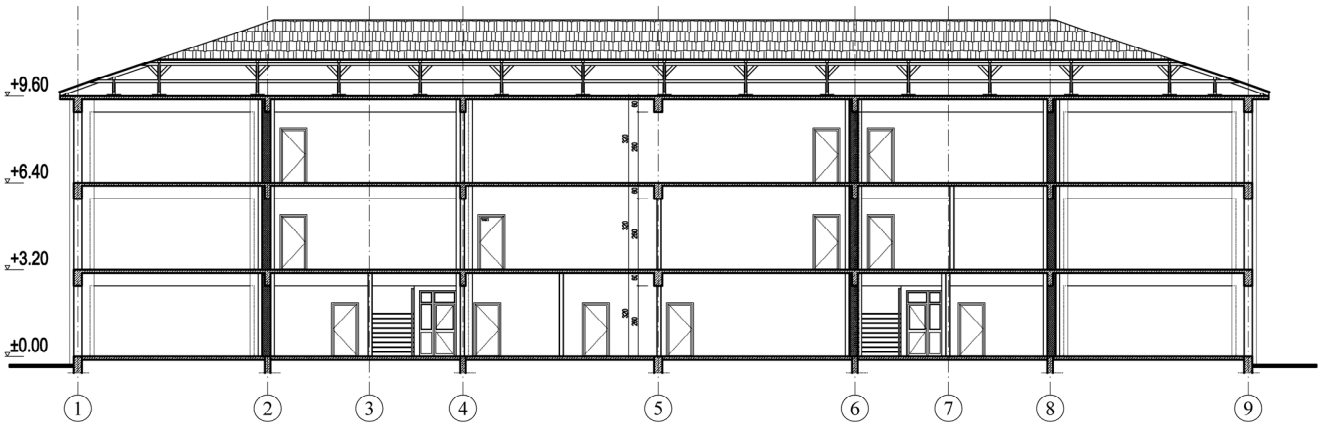

Figure 9. The architectural cross-section of the school building.

Investigations revealed that the concrete strength did not meet the minimum requirements stipulated by the 2007 Turkish Earthquake Code [19], and the building's earthquake performance did not satisfy the specified standards. Accordingly, the retrofit process was implemented, which involved adding new shear walls between frame columns and jacketing the columns with a jacketing thickness of 15 cm. A total of 11 shear walls were added, each 30 cm thick: 5 in the long direction and 6 in the short direction. The new members were anchored to the existing frame columns using epoxy-based chemicals. Relevant drawings illustrate how the jacketed columns connected to the existing ones [20]. The concrete and reinforcement quality used in the strengthening elements were C30 and S420, respectively.

Table 4 gives the dimensions of the structural elements after strengthening, according to the existing floor plans. The school building's existing beams and two-way slab floors did not undergo a strengthening process. Local strengthening was applied to the foundation system. The slab plans of the retrofitted building are shown in Figures 10–12.

Table 4. Dimensions of school building structural elements.

Structural Element	Dimension
Columns (cm × cm)	60 × 80–60 × 90–80 × 70–90 × 60
Beams (cm/cm)	20/60–30/60
Two-way slabs (cm)	12
Shear walls (cm)	30

In 2017, following the retrofitting work, a technical report was prepared detailing the damages caused by the metro tunnel excavation and the necessary precautions to take [18]. The observations of the load-bearing system elements of the school building yielded the following findings [20]:

- Horizontal, vertical, and diagonal cracks were observed on the surfaces of the reinforced concrete shear walls. Upon removing and examining the plaster layer, some diagonal cracks on the reinforced concrete surface were found to be micro-width only;

- No visible cracks or damage were observed in the retrofitted concrete columns;
- Cracks caused by settlement were observed in the reinforced concrete beams and were significant enough to adversely affect the shear strength of the beams. It was concluded that these members were at risk of potential collapse;
- Cracks were observed on the surfaces of the reinforced concrete slabs, most of which were hairline cracks, with visible deflection observed in some slabs.

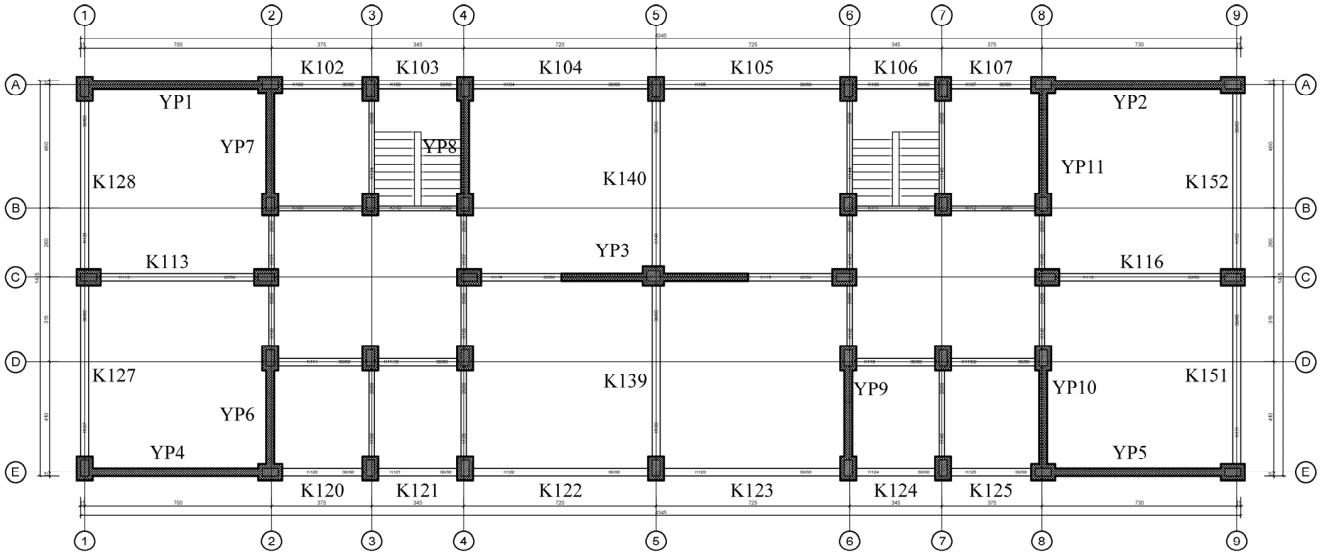

Figure 10. The structural layout of the +3.20 level slab, featuring jacketed columns and added shear walls for strengthening between frame columns.

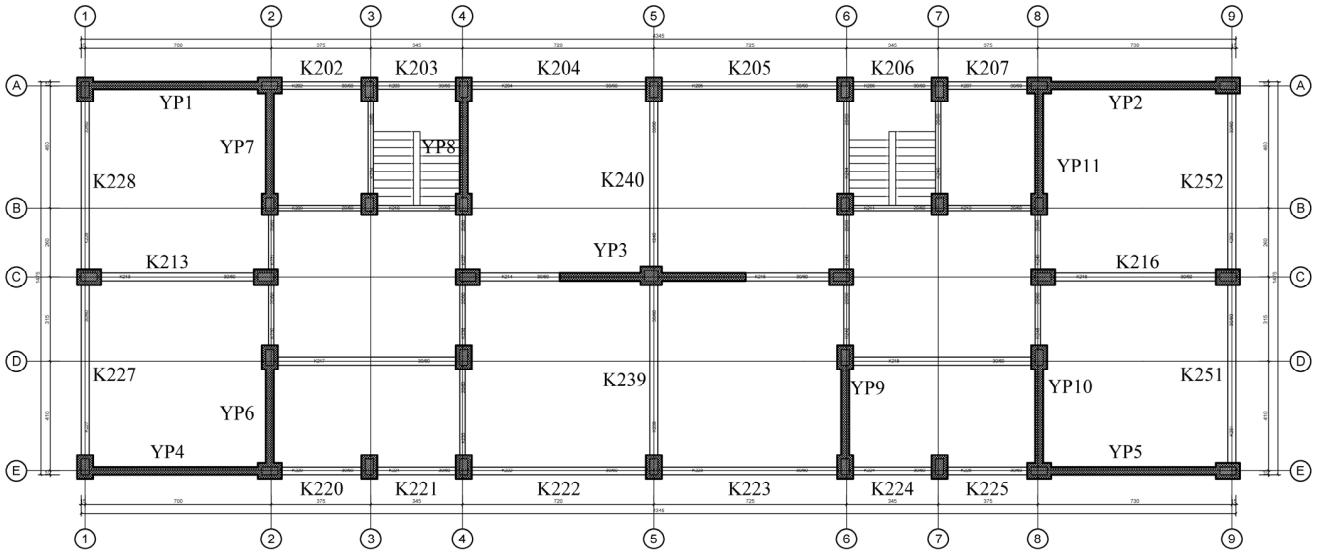

Figure 11. The structural layout of the +6.40 level slab, featuring jacketed columns and added shear walls for strengthening between frame columns.

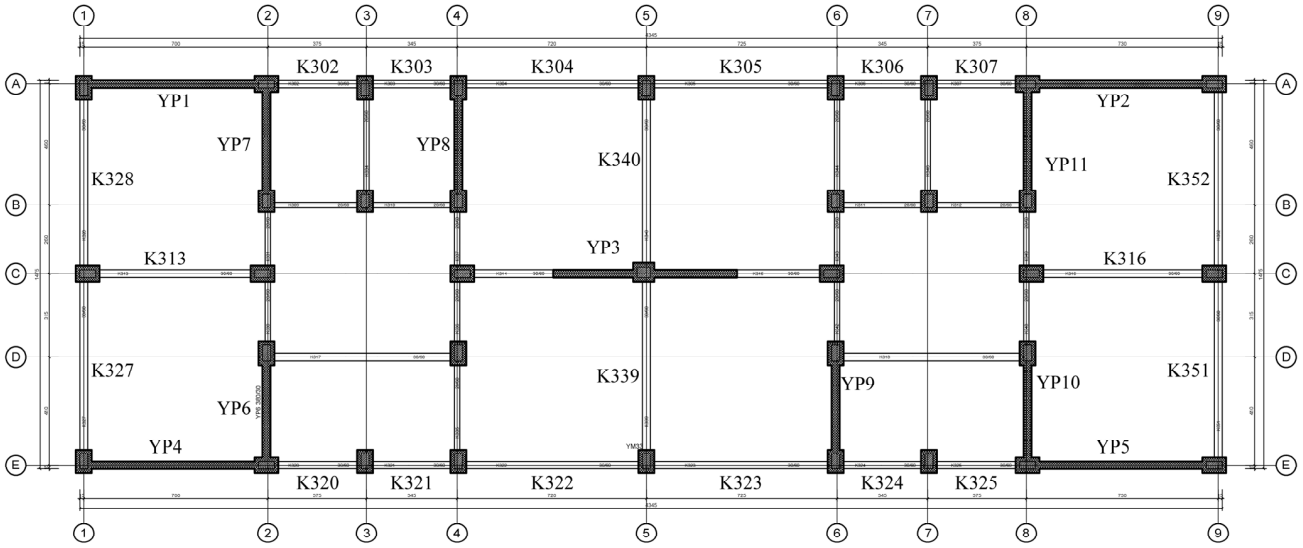

Figure 12. The structural layout of the +9.60 level slab, featuring jacketed columns and added shear walls for strengthening between frame columns.

SAP2000 Analysis Model Principles for School Building

This study aimed to verify the damage to the school building by considering the settlement measured in the field. For this reason, a SAP2000 analysis model for the retrofitted case was created based on the floor plans (Figure 13). The dead load was set at 4 kN/m^2 for the slabs and 2 kN/m^2 for the roof slab, while the live load was set at 5 kN/m^2 for the slabs and 2 kN/m^2 for the roof slab.

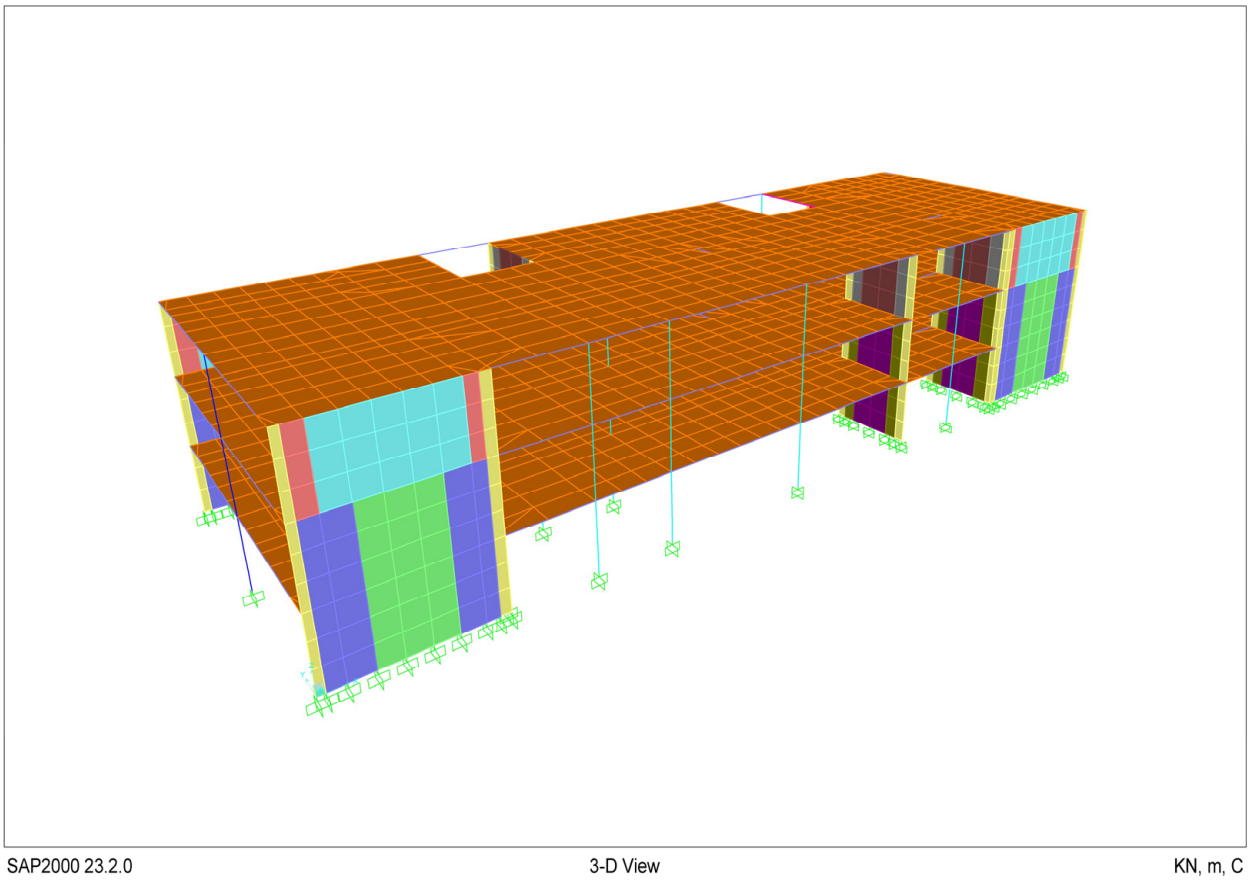

Figure 13. SAP2000 3D analysis model.

As previously mentioned, calculations were conducted in stages to determine the deformations that would occur in the buildings along the route before the metro tunnel excavation began. As a result of these calculations, precautions were taken to keep buildings in critical condition. Given that the school building was deemed to be in critical condition during the empirical calculation phase, measurement devices (reflectors) were placed around the periphery of the school building to monitor deformations during the metro tunnel excavation (Figure 14). The data obtained from these measurement devices were utilized as vertical displacements in the analysis model created in SAP2000 (Table 5).

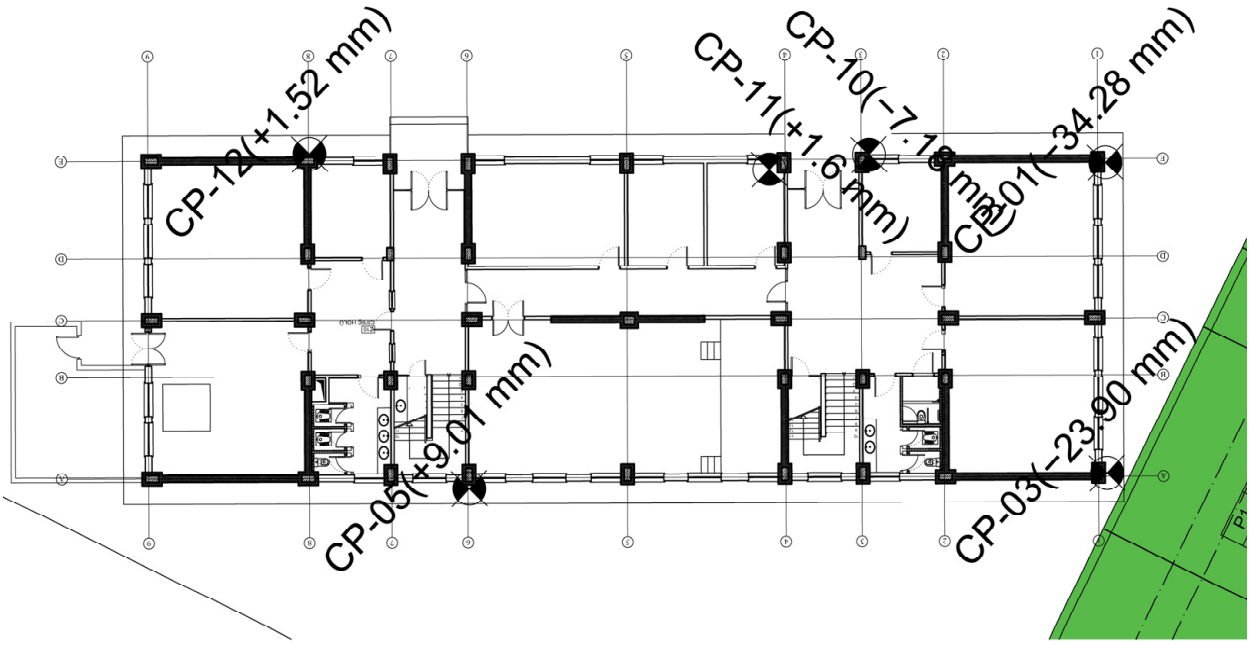

Figure 14. Layout plan of measurement devices (reflectors).

Table 5. Settlement values obtained from field measurements.

Measurement Devices	Displacement (ΔZ (mm))
CP-01	−35
CP-03	−24
CP-05	9
CP-10	−7
CP-11	2
CP-12	2

It was assumed that the columns and shear walls of the building were fixed to the foundation. The vertical displacements obtained from measurement devices (Table 5) were applied to these supports, and a pushover analysis in the vertical direction was conducted. A nonlinear material model was defined for the concrete and reinforcement (Figures 15 and 16). The lumped plastic behavior model and the distributed plasticity model were utilized to represent the nonlinear behavior of the beams. The distributed plastic behavior model was applied to the shear walls and defined as a multi-layer shell element. Each support was pushed to its defined "target displacement", and the beam plastic hinge outputs corresponding to the vertical displacement demand were obtained. Additionally, the concrete and reinforcement strain for the shear walls were evaluated. No plastic hinge formation was observed in the columns; therefore, a linear material model was used.

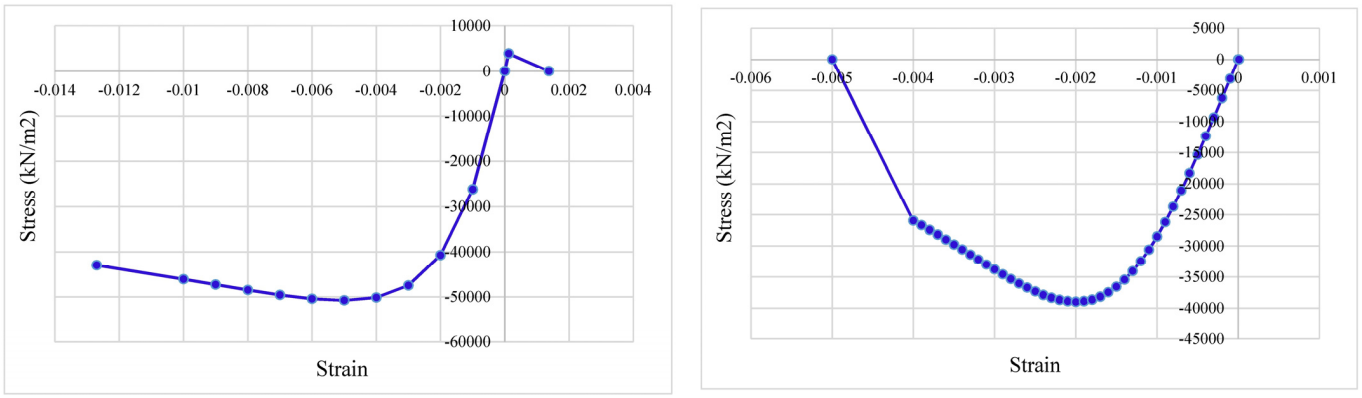

(**a**) (**b**)

Figure 15. Nonlinear material model for the school building: (**a**) confined concrete; (**b**) unconfined concrete.

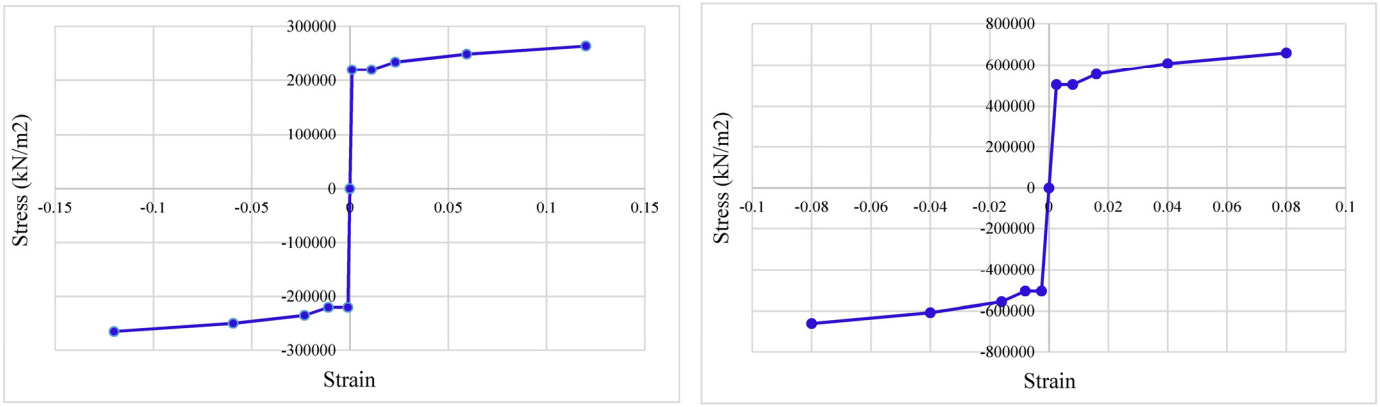

(**a**) (**b**)

Figure 16. Nonlinear material model for the school building: (**a**) S220 reinforcement class; (**b**) S420 reinforcement class.

The elements in the analysis model were created based on information gathered from the field and specified in the inspection report. During field inspections, cracks were observed on the plaster surface of the columns; however, no crack formation affecting the reinforced concrete column sections was noted. Significant effects were observed on the beams and retrofitted shear walls. In light of this information, the following can be stated:

- In TBSC 2018, cases where the ratio of the largest shear wall arm length in the plan to the total shear wall height does not exceed 1/2 can be modeled as an equivalent frame element. Since the shear walls of the school building did not meet this condition, they were modeled as a multi-layer shell element for the nonlinear finite element analysis (Figure 17). In the modeling phase, the reinforcement details of the shear wall boundary zones were defined as specified in the drawings, and a confined concrete model was used in these areas. An unconfined concrete model was defined for regions outside the shear wall boundary zones;
- A nonlinear material model was defined for the reinforced concrete beams. Plastic hinges were defined at the beam support faces in the column–beam joint areas and throughout the beam span areas. Due to the vertical displacement, an increase in tensile force in the beams is to be expected. Therefore, plastic hinges should be defined at the beam support faces in the column–beam joint areas and along the beam span areas. A fiber hinge type was used to observe the effects of axial forces on the beam. The fiber model exhibiting deformation-controlled behavior was defined for P-M2-M3 (Figure 18). This approach aimed to verify the tensile effects observed in the

photographs of beam damage. Additionally, shear hinges were defined to assess the effects of the shear forces in the beams occurring due to the vertical displacement. The behavior of these shear hinges was force-controlled (brittle behavior). A hinge was formed when the beam reached its shear capacity, indicating collapse of the element. A lumped plasticity model using the Caltrans model to evaluate the beams with shear hinges was defined for the M3 direction (Figure 18). These hinges also exhibited deformation-controlled behavior. The beams where shear and M3 hinges were defined include K113, K213, K313, K116, K216, K316, K139, K239, 339, K140, K240, and K340 (Figure 19). For all other beams, a fiber model was defined. Nonlinear material models for concrete and reinforcement were also applied in these sections;

- A linear material model was used for the columns and slabs.

The effective section stiffness multiplier for structural elements was obtained as specified in TBSC 2018 (Table 4.2) [21].

The school building's beams were not strengthened, and reinforcement drawings were not available for these structural elements. It was assumed that the school building had been designed and constructed according to the 1975 Turkish Earthquake Code [22]. Thus, the reinforcement details were determined based on the minimum reinforcement requirements specified in this code; the minimum longitudinal reinforcement ratio (ρ_{min}) in beams for St I (S220) is 0.005. The minimum transverse reinforcement was also calculated according to this code.

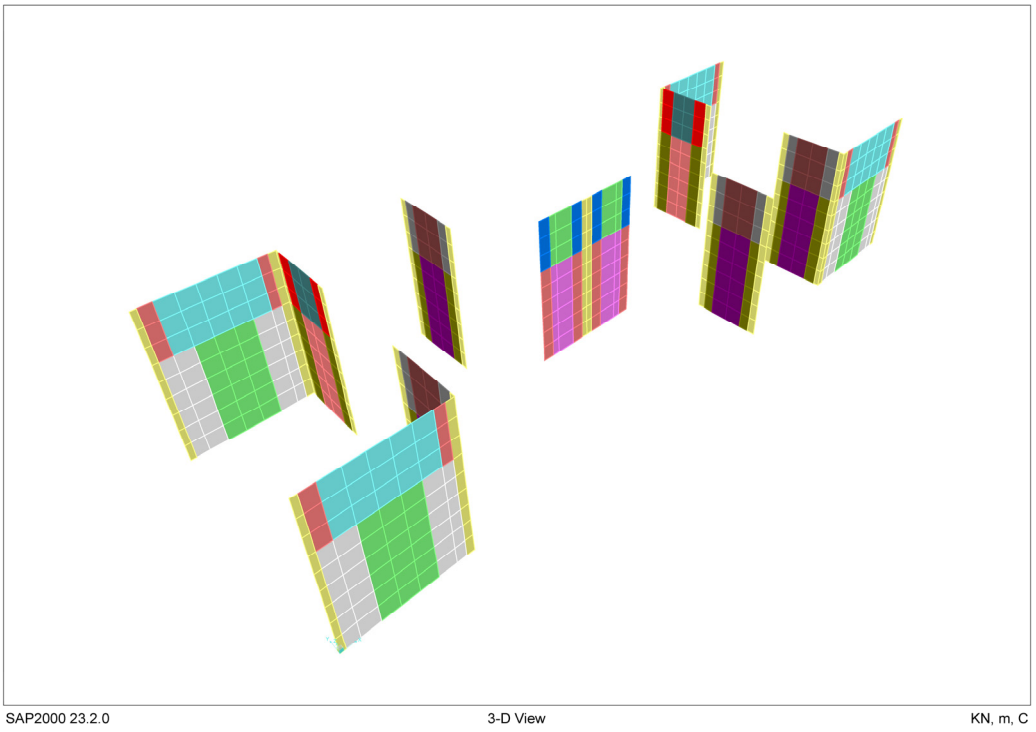

Figure 17. Reinforced concrete shear walls modeled as multi-layered shell elements for the nonlinear finite element analysis.

The system included four types of reinforced concrete columns (Table 4). Due to the low strength of the concrete, the existing parts of the columns were neglected, and the columns were modeled as box column sections during the modeling phase. The reinforcement drawings for these columns are available.

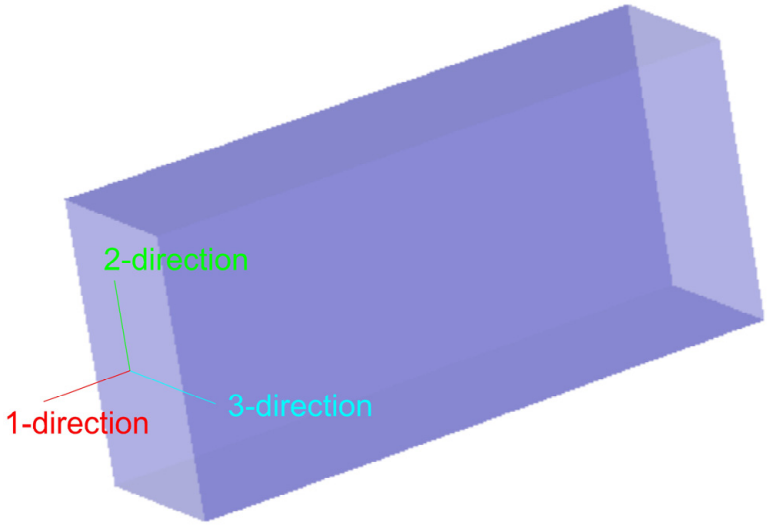

Figure 18. Beam section local axes.

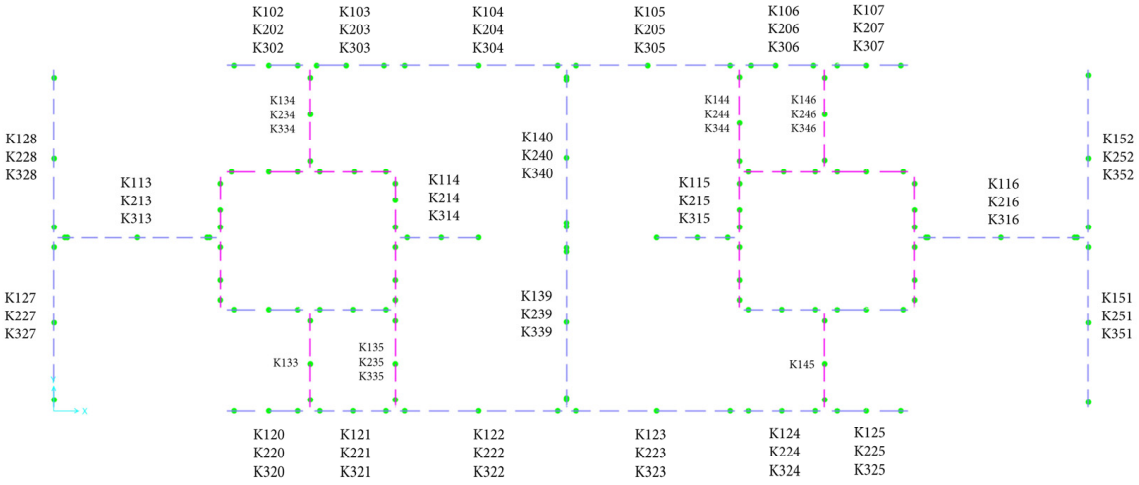

Figure 19. SAP2000 analysis model floor plan, beam plastic hinge layout.

3. Results

The static pushover analysis results were obtained to assess whether the reinforced concrete structural elements in the system were consistent with the damages reported from the field. As mentioned, the columns were modeled as linear frame elements, since no damage was observed in the field. According to the data obtained from the analysis model, the columns remained within the limits of linear elastic behavior.

In the field report, it was stated that the cracks were present in the frame beams. Comments suggested that these cracks could reduce the shear capacity of the beams and potentially lead to failure if the capacity were exceeded. In order to evaluate whether the shear capacity had been reached, shear hinges were defined for the beams K113, K116, K139, K140, K213, K216, K239, K240, K313, K316, K339, and K340. No shear hinge formation was observed in these beams. Shear forces in the beams were generated under gravity load. The target displacement did not produce significant shear forces in the beams. Figure 20 shows the shear force diagram for the C-axis beams. The diagram showing shear force versus step number is given in Figure 21 for beam K213 under both gravity load and target displacement.

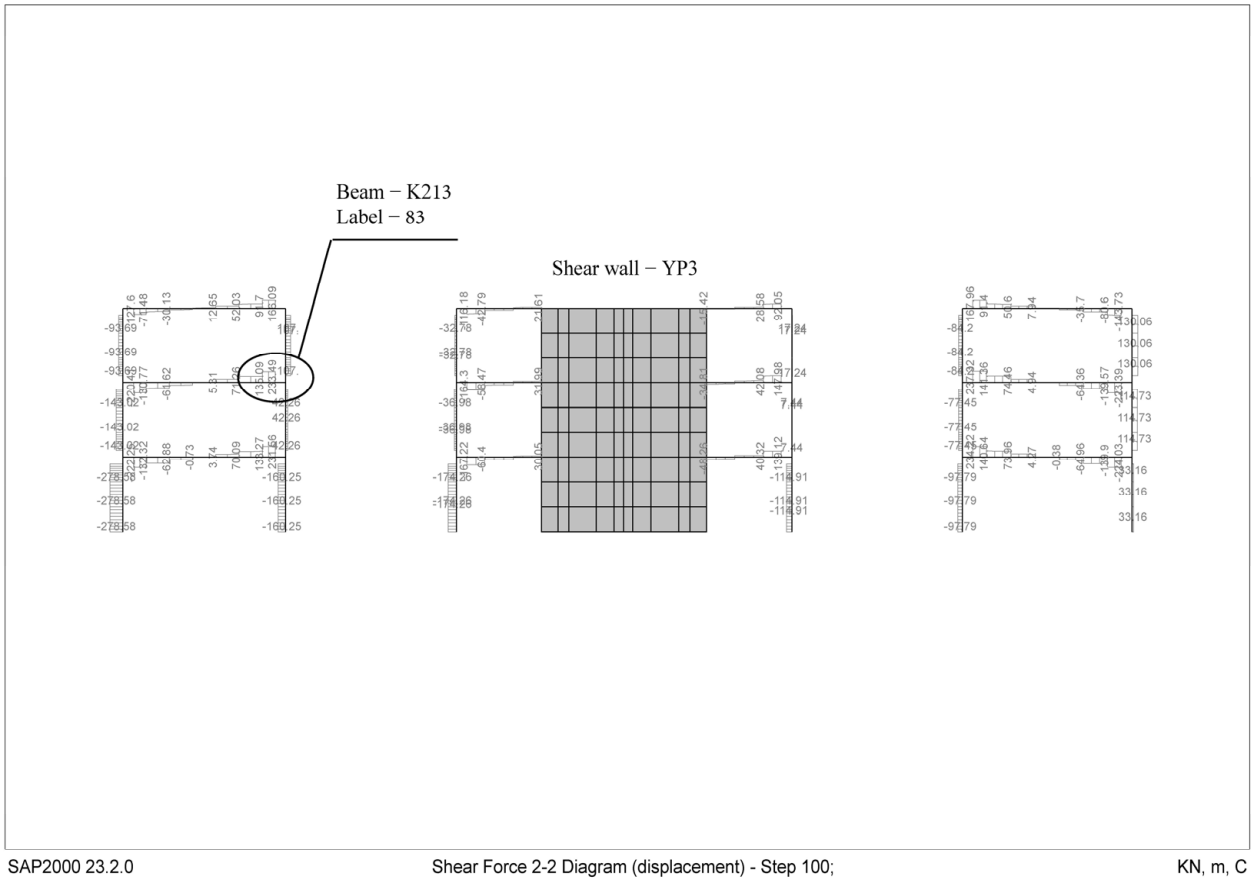

Figure 20. The shear force diagram of the beam for axis C.

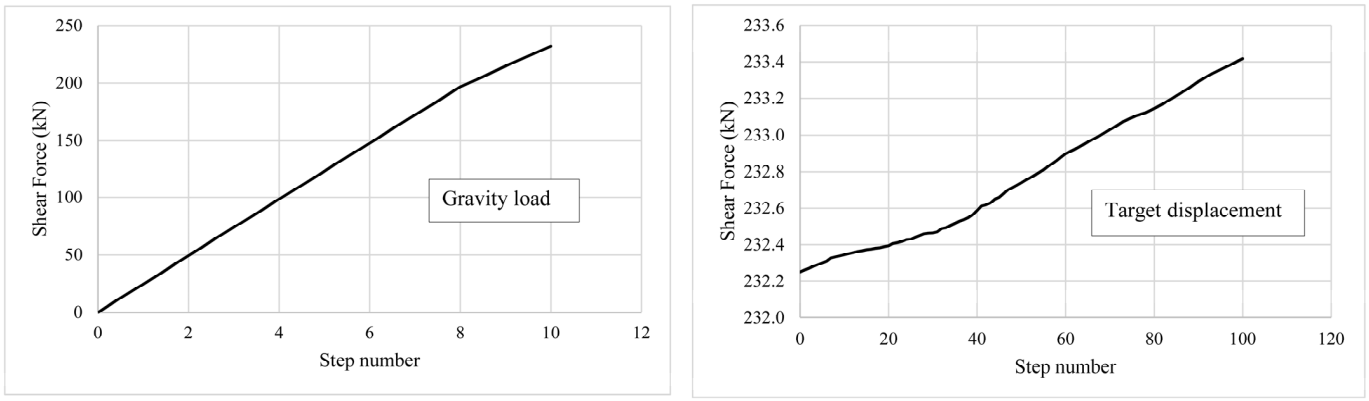

(**a**) (**b**)

Figure 21. The shear force—step number diagram for beam K213: (**a**) under gravity load; (**b**) under target displacement for vertical pushover analysis.

Additionally, tensile forces acting on the beams are expected to increase under vertical displacement. Therefore, tensile force is another potential cause of crack formation in the beams. Fiber hinges were defined to observe the axial force's effects on the beams. Figure 22 shows the axial force diagram for the beams with defined fiber hinges under target displacement for axis E. The axial force in the beams increased until the solution reached the target displacement value. The diagram of axial force versus step number for beam K320 is provided in Figure 23.

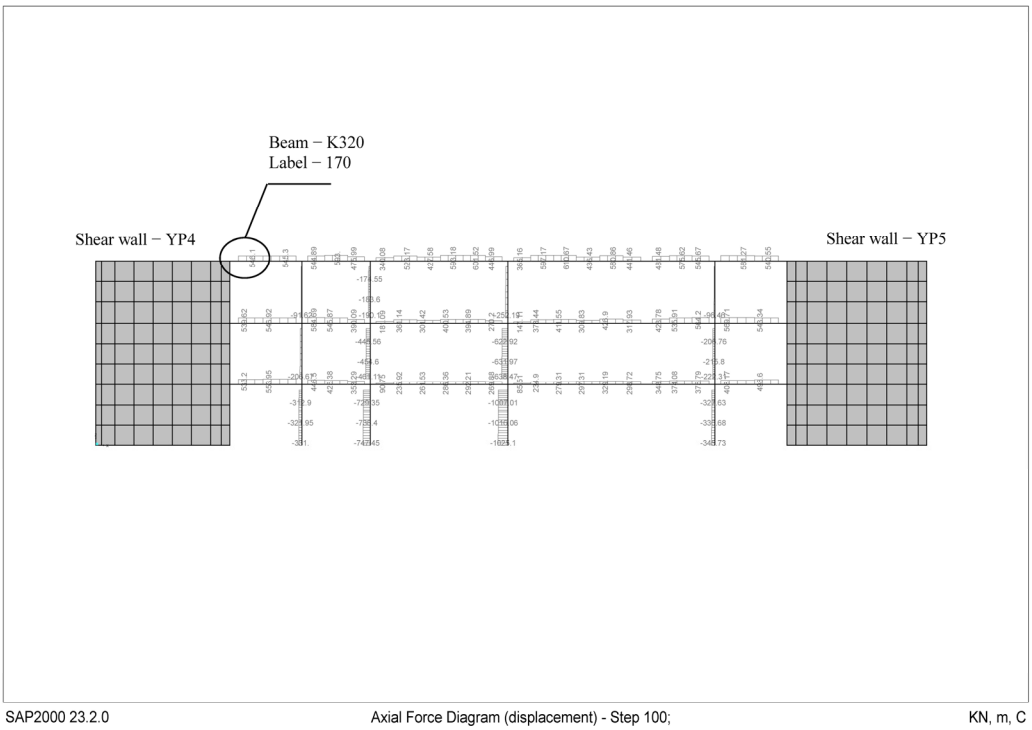

Figure 22. The axial force diagram of the beam for axis E.

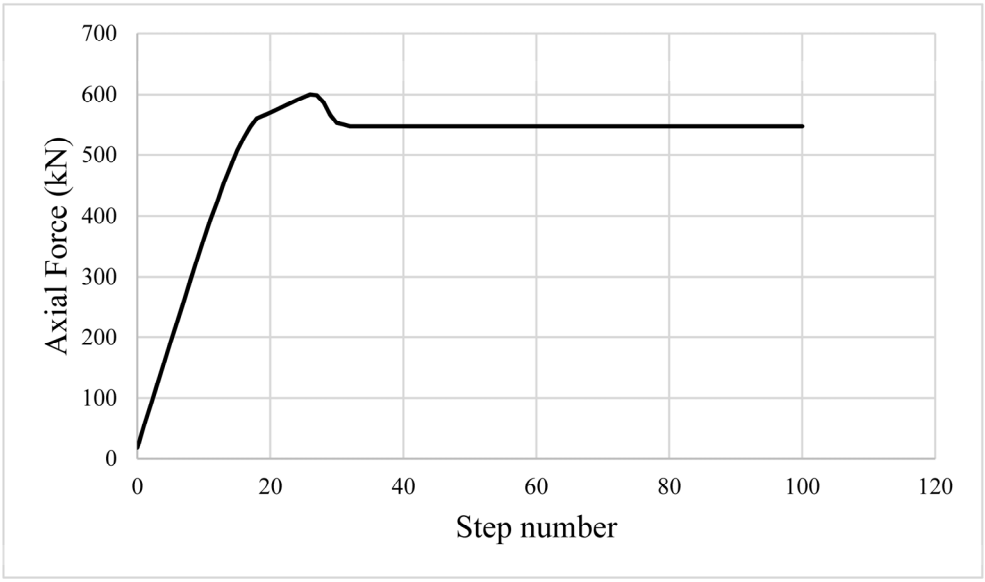

Figure 23. The axial force–step number diagram for beam K320 under vertical settlement.

For the pushover analysis, the plastic hinges utilizing both the Caltrans and fiber models for the beams were evaluated according to TBSC 2018 [21]. Plastic rotation control was conducted for the Caltrans model plastic hinges, while total strain control was performed for the plastic hinges using the fiber model. The section damage states for each reinforced concrete beam, as specified in TBSC 2018, were determined (Figure 24) [21]. Accordingly, the distribution of cross-sectional damage in the reinforced concrete beams at each floor level is presented in Table 6. The beams K113, K116, K139, and K140 at elevation +3.2; K213, K216, K239, and K240 at elevation +6.4; and K316, K320, K339, and K340 at elevation +9.6 were categorized in the significant damage zone. The damage assessment was based on each element's most severely damaged section [21].

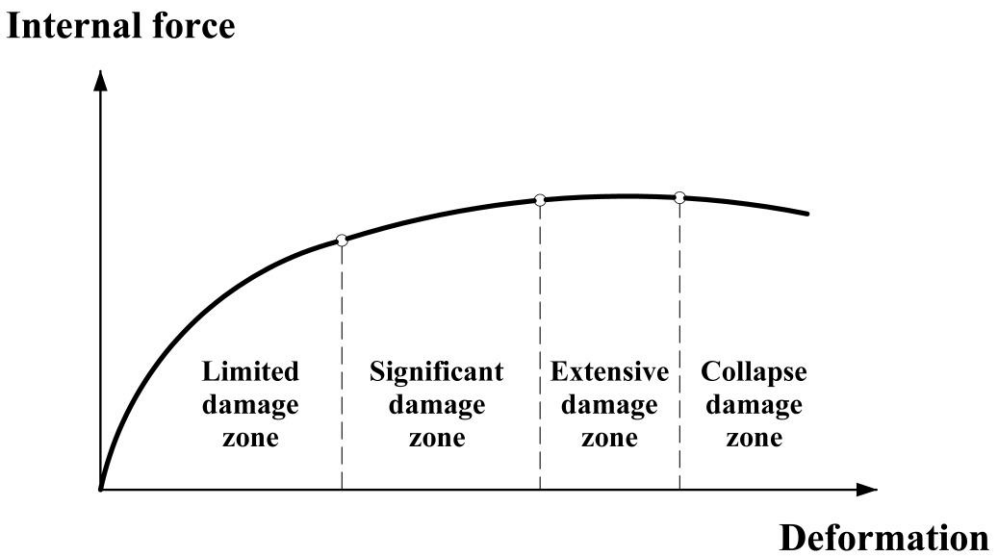

Figure 24. Section damage states.

Table 6. Damage state distribution of reinforced concrete beams.

Elevation	Limited Damage	Significant Damage	Extensive Damage	Collapse
+3.2	90.9%	9.1%	-	-
+6.4	90.0%	10.0%	-	-
+9.6	90.0%	10.0%	-	-

The reinforced concrete shear walls, defined as multi-layer shell elements for the nonlinear finite element analysis, were subjected to strain control. In the analysis model, the concrete strain in the shear walls was 0.000387 and the reinforcement strain was 0.001481 (Table 7). The minimum damage performance level limits specified in the TBSC 2018 are 0.0025 for concrete (ε_c) and 0.0075 for reinforcement steel (ε_s) [21]. Accordingly, the reinforced concrete shear walls remained within the limited damage zone.

Table 7. The concrete and reinforcement strain values for shear walls of the school building.

Shear Wall Name	ε_c	ε_s
YP1	0.000197	0.000197
YP2	0.000106	0.000145
YP3	0.000232	0.000204
YP4	0.000229	0.001481
YP5	0.000140	0.000236
YP6	0.000318	0.000318
YP7	0.000161	0.000133
YP8	0.000387	0.000394
YP9	0.000157	0.000157
YP10	0.000146	0.000147
YP11	0.000096	0.000030

4. Discussion

Tunnel constructions for rapid public transportation with rail systems in urban areas can cause damage to existing structures. It is crucial to conduct studies to address this significant issue. Displacements occurring on the ground surface due to metro tunnel excavations can impact buildings along the route. Creating a numerical analysis model to investigate these effects for all buildings within the affected area is not feasible [23,24]. For this reason, Mair et al. (1996) [9] proposed an evaluation method consisting of three stages:

preliminary assessment, second-stage assessment, and detailed assessment. Parametric calculation methods are available for the preliminary and second-stage assessments; however, detailed assessment requires a 3D numerical analysis model.

In this study, a school building was selected to apply the three-stage assessment method described above. The "greenfield" analysis approach was implemented using Plaxis2D for the preliminary assessment stage, and the displacements on the ground surface were obtained. The vertical displacement value obtained from the analysis model was 79 mm, exceeding the allowable value of 10 mm proposed by Mair et al. (1996) [9] for the preliminary assessment. Consequently, the second-stage assessment was initiated.

The "greenfield" analysis conducted using PLAXIS 2D indicated that the expected maximum vertical displacement value at the school building's location was 79 mm. However, the maximum displacement value obtained from the measurement devices placed at the school building site was 35 mm. The building stiffness affects the settlement curve and the building [8]. Since the soil–structure interaction is neglected in the PLAXIS 2D analysis model, the assessments based on the expected displacement value are overly conservative [3].

In the second-stage assessment, the settlement curve for the school building was deemed to be appropriate, based on the "greenfield" analysis model, and tensile strain control was conducted for the hogging and sagging regions of the building. The analysis results in Table 3 were compared with the allowable tensile strains in Table 1, leading to the decision to proceed to the detailed assessment stage. In this phase, a SAP2000 analysis model of the existing school building was created. The literature review revealed deficiencies in the modeling principles of 3D numerical analysis for buildings subjected to vertical settlement effects due to tunnel construction. This study aimed to establish modeling principles for the SAP2000 finite element model generated during the detailed assessment phase.

During the detailed evaluation phase, a vertical pushover analysis was developed as a new numerical approach to address settlement-related problems in buildings and verify causes of damage. The "target displacements" used for the vertical pushover analysis were derived from measurements from devices installed at the school building. Therefore, the field survey report for the existing school building was utilized. According to the results obtained the modeling principles, the school building remained within the damage limits specified in the relevant codes [21].

5. Conclusions

The damage evaluation of existing buildings induced by tunnel excavation is considered in this study. A new approach is proposed, modeling principles of pushover analysis by separately evaluating each structural element of a building under the effect of vertical displacement. The following findings were observed during the generation of the vertical pushover analysis model:

- Linear modeling of reinforced concrete shear walls resulted in tensile forces exceeding the capacity of the columns. Therefore, these types of wall should be modeled using multi-layered shell elements, with a fiber model (cross-sectional fiber model) defined for these elements;
- The columns were modeled as nonlinear elements, and a Caltrans model plastic hinge was defined; however, no hinge formation was observed. Since the field conditions were verified, it was decided to model the columns linearly;
- The effects of tensile forces on beams increased until they reached the target displacement. This indicates that tensile forces are significant in the beams of a building experiencing vertical settlement effects. Plastic hinges should be defined at the beam–column

joint and beam-span areas in beams subjected to tensile forces, and a fiber hinge used to examine the nonlinear behavior of structural elements under tensile forces;

- In beams where shear effects were observed, shear hinges were defined in order to identify elements that reached their shear capacity. The system did not converge in an element where both shear and fiber hinges are used simultaneously in the same location. Therefore, plastic hinges using the Caltrans model should also be established in beams with defined shear hinges in order to assess the bending effects accurately. The shear forces in the beams subjected to vertical displacement reached high values under gravity load. The shear forces did not vary significantly in the steps where target displacement was effective.

This study focused on modeling a school building that had already received investigation results, establishing the principles of vertical pushover analysis in terms of reliability. The compatibility of the school building's field measurements with the model results shows the reliability of the given modeling principles.

Author Contributions: Conceptualization, E.E.L.A. and K.G.; methodology, K.G.; software, E.E.L.A.; validation, E.E.L.A.; formal analysis, E.E.L.A.; investigation, E.E.L.A. and K.G.; resources, E.E.L.A. and K.G.; data curation, E.E.L.A. and K.G.; writing—original draft preparation, E.E.L.A. and K.G.; writing—review and editing, E.E.L.A. and K.G.; supervision, K.G.; project administration, E.E.L.A. and K.G. All authors have read and agreed to the published version of the manuscript.

Funding: This research received no external funding.

Data Availability Statement: Data are contained within the article.

Acknowledgments: The authors would like to express their gratitude towards Yasin Fahjan for his contributions to this research.

Conflicts of Interest: The authors declare no conflicts of interest.

References

1. Ayasrah, M.; Qui, H.; Zhang, X.; Daddow, M. Prediction of ground settlement induced by slurry shield tunneling in granular soils. *Civ. Eng. J.* **2020**, *6*, 2273–2289. [CrossRef]
2. Liu, J.; Huang, X.; Li, K.; Dai, Y.; Ma, W. Numerical investigation of existing tunnel deformation induced by basement excavation considering the unloading ratio. *Appl. Sci.* **2023**, *13*, 9457. [CrossRef]
3. Zhao, J. Numerical Modeling and Uncertainty Analysis of Tunneling and Deep Excavation-Induced Structural Damage. Ph.D. Thesis, University of California, Berkeley, CA, USA, 2023.
4. Haji, T.K. Evaluating the Effects of Tunnel Construction on Buildings. Ph.D. Thesis, University of Nottingham, Nottingham, UK, 2017.
5. Liu, W.; Liang, J.; Xu, T. Tunnelling-induced ground deformation subjected to the behavior of tail grouting materials. *Tunn. Undergr. Space Technol.* **2023**, *140*, 105253. [CrossRef]
6. Boldini, D.; Losacco, N.; Bertolin, S.; Anorosi, A. Finite element modeling of tunneling-induced displacements on framed structures. *Tunneling Undergr. Space Technol.* **2018**, *80*, 222–231. [CrossRef]
7. Giardina, G.; Losacco, N.; DeJong, M.J.; Viggiani, G.M.; Mair, R.J. Effect of soil models on the prediction of tunneling-induced deformations of structures. *Proc. Inst. Civ. Eng. Geotech. Eng.* **2019**, *173*, 379–397. [CrossRef]
8. Li, Y.; Zhou, G.; Li, T.; Tang, C.; Gong, B.; Wang, K. Influence of tunnel excavation on the deformation of a frame building. *Buildings* **2023**, *13*, 810. [CrossRef]
9. Mair, R.J.; Taylor, R.N.; Burland, J.B. Prediction of ground movements and assessment of risk of building damage due to bored tunneling. In Proceedings of the Geotechnical Aspects of Underground Construction in Soft Ground, London, UK, 15–17 April 1996; AA Balkema: Amsterdam, The Netherlands, 1996; pp. 713–718.
10. Peck, R.B. Deep excavations and tunneling in soft ground. In Proceedings of the 7th International Conference on Soil Mechanics and Foundation Engineering, Mexico City, Mexico, 25–29 August 1969; pp. 225–290.
11. Schmidt, B. Settlement and Ground Movements Associated with Tunneling in Soil. Ph.D. Thesis, University of Illinois, Urbana, IL, USA, 1969.
12. Gugliemetti, V.; Grasso, P.; Mahtab, A.; Xu, S. (Eds.) *Mechanized Tunneling in Urban Areas*; Taylor & Francis Group: London, UK, 2007.

13. Burland, J.B.; Wroth, C.P. Settlement of buildings and associated damage. In Proceedings of the Conference Settlement of Structures, Cambridge, UK, April 1974; Pentech Press: London, UK, 1974; pp. 611–654.
14. Loganathan, N. *An Innovative Method for Assessing Tunneling-Induced Risks to Adjacent Structures*; Parsons Brinckerhoff Inc.: New York, NY, USA, 2011.
15. Boscardin, M.D.; Cording, E.J. Building Response to excavation-induced settlement. *ASCE J. Geotech. Eng.* **1989**, *115*, 1–21. [CrossRef]
16. Addenbrook, T.I.; Potts, D.M.; Puzrin, A.M. The influence of pre-failure soil stiffness on the numerical analysis of tunnel construction. *Geotechnique* **1997**, *47*, 693–712. [CrossRef]
17. Efe, F.; Kuçukoglu, M.; Nurnur, H. Design and construction of N1 shaft for Dudullu-Bostanci metro line. In *Tunnels and Underground Cities: Engineering and Innovation Meet Archaelogy, Architecture and Art*, 1st ed.; CRC Press: London, UK, 2020.
18. Aydoğan, M.; Çelik, M. *Istanbul İli, Ümraniye İlçesi, Dudullu Imam Hatip Ortaokulu Binasında Gözlenen Hasarlar ve Alınması Gereken Önlemler Hakkında Teknik Rapor*; Istanbul Technical University, Civil Engineering Department: Istanbul, Turkey, 2017. (In Turkish)
19. *Specification for Buildings to be Built in Seismic Zones*; Ministry of Public Works and Settlement Government of Republic of Turkey: Ankara, Turkey, 2007.
20. Alhan, C. *Istanbul Ili, Ümraniye İlcesi, Dudullu İmam Hatip Ortaokulu B Blok Binasında Zemin Oturmalarının Etkisinin Yapı Mühendisliği Açısından Değerlendirilmesi Hakkında Teknik Rapor*; Istanbul University, Cerrahpaşa Faculty of Engineering, Civil Engineering Department: Istanbul, Turkey, 2023. (In Turkish)
21. *Turkish Building Seismic Code*; Turkish Government Ministry of Interior Disaster and Emergency Management Presidency: Ankara, Turkey, 2018.
22. *Specifications for Structures to be Built in Disaster Areas*; Turkish Government Ministry of Reconstruction and Resettlement: Ankara, Turkey, 1975.
23. Zhang, X.; Qu, H.; Xu, Y.; Zhang, L.; Zhang, Z. Investigating the damage to masonry buildings during shield tunneling: A case study in Hohhot Metro. *Eng. Fail. Anal.* **2024**, *160*, 108147. [CrossRef]
24. Meschke, G.; Breitenbücher, R.; Freitag, S.; König, M.; Thewes, M. (Eds.) *Interaction Modeling in Mechanized Tunneling*; Springer Nature: Berlin/Heidelberg, Germany, 2023.